Co-Channel Interference Mitigation Detectors for Multirate Transmission in TD-CDMA Systems

Piero Castoldi, *Associate Member, IEEE*, and Hisashi Kobayashi, *Fellow, IEEE*

***Abstract*—In this paper, we address the problem of downlink detection in a mobile radio time division/code division multiple access multirate communication system employing a linear modulation. We focus on the detection of a group of intracell codes (ranging from a single one to all the active codes) rejecting both interference coming from the complementary set of undesired intracell codes and co-channel intercell interference. We investigate efficient implementations of linear nonadaptive multiuser detection realized by either joint or separate intersymbol interference and multiple access interference (MAI) mitigation using the zero-forcing or minimum mean square error criteria.**

The proposed detection schemes employ a tunable-complexity structured description of the MAI for the purpose of detection and interference mitigation. Specifically, the receivers always envision an intracell interference mitigation and data detection capability, while intercell interference is treated differently depending on operating environments. If a statistical description of the intercell interference is available, the receiver realizes group detection in the presence of possibly nonwhite Gaussian noise. Soft hand-over procedures are also proposed wherein direct suppression of intercell interference is possible as well as group detection of the data of the neighboring cells.

A unified and finite complexity implementation of the proposed detection schemes based on a sliding window formulation is provided. The numerical results validate the proposed receiver structures showing that a structured description of the observation always leads to a detector with superior performance.

***Index Terms*—Code division multiaccess, interference suppression, land-mobile radio cellular systems.**

I. Introduction

THE THIRD-GENERATION mobile radio system will be based on direct sequence code division multiple access (DS-CDMA). One of the proposed duplexing techniques to be employed for high data rate applications and picocell coverage is the time division duplex (TDD) mode, which uses separate time slots for the uplink and downlink streams [1], [2]. The TDD mode uses orthogonal variable spreading factor (OVSF) channelization codes [2], allowing for a large flexibility in data transmission rate.

Multirate CDMA transmission is a relatively new topic for research and some efforts have recently started to investigate receivers for such systems [3]–[7]. Since multiple codes may be assigned to the same mobile user, the mobile receiver should be able to detect the data carried by a subset of the active codes used in the current time slot. An intracell signal in the downlink is modeled as a synchronous CDMA system where all codes experience the same (possibly multipath) propagation channel. A generic interferer coming from another cell in the downlink can be described by the same structure as the intracell signal. Hence, intercell interferers are asynchronous to each other and with respect to their respective intracell signal. The base station (BS) specific scrambling sequences used to "mask" every intracell beam of OVFS codes are short, i.e., their duration is at most a few symbol intervals, whose relevant observation window is assumed to have stationary statistics [8].

In this paper, we investigate the downlink group detection of the data carried by a set of codes (whose cardinality varies from one to the totality of all active codes) rejecting both the interference due to the complementary set of intracell codes and that coming from other cells (co-channel intercell interference). Multistage detectors employing a combined linear and nonlinear interference suppressor have been recently reported [9], [10]. Our focus, instead, is on "all-linear" detectors based on the zero-forcing (ZF) or minimum mean square error (MMSE) criterion to counteract intersymbol interference (ISI) by equalization and both intracell and intercell multiple access interference (MAI) by interference mitigation.

Among the seminal papers that deal with the mentioned linear detectors we recall [10]–[13], which focus on a single-rate CDMA system, whereas [3] presents an introductory investigation of either joint and separate ISI equalization and intracell MAI mitigation using ZF criterion in a multirate system. The present work extends previous studies [3]–[5] and [10]–[13], by defining a unique framework for joint or separate ISI linear equalization and *both* intracell and intercell linear interference mitigation in a multirate system. For the receiver design we rely on the fact that detection performed by a mobile station (MS) can always exploit explicit knowledge concerning all the intracell codes currently assigned to a time slot, because the codes destined to a specific MS are notified using a control channel [1], while the others can be determined by processing the midamble of the packet [2]. Hence, the observation model always includes a "structured" description of the intracell signals. Consequently, the direct intracell mitigation feature is always set "on," while different options are available for co-channel intercell interference suppression.

A statistical description of the intercell interference allows us to employ receivers derived in [5] by augmenting their capability to deal with nonwhite background noise, which

Manuscript received December 12, 2000; revised August 1, 2001 and October 20, 2001. This work was supported in part by CNR in the framework of Progetto Finalizzato *Madess II*, subproject "CDMA Interference Mitigation Receiver (CIMR)," and by the New Jersey Center for Wireless Telecommunications (NJCWT).

P. Castoldi is with the Scuola Superiore Sant'Anna, di Studi Universitari e Perfezionamento, 56127 Pisa, Italy (e-mail: castoldi@sssup.it).

H. Kobayashi is with the Department of Electrical Engineering, Princeton University, Princeton, NJ 08544 USA (e-mail: hisashi@ee.princeton.edu).

Publisher Item Identifier S 0733-8716(02)01008-9.

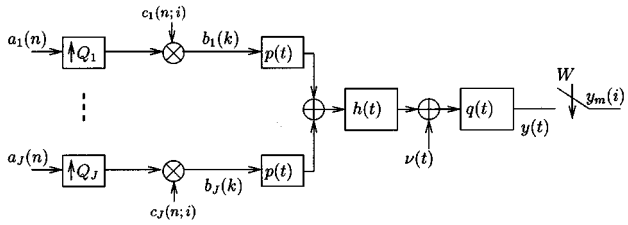

Fig. 1. Model of the considered transmission system.

characterizes the disturbance due to both intercell interference and additive white Gaussian noise (AWGN). In a soft hand-over scenario the parameters of the neighboring cell(s) must be known to the MS. The MS can realize a direct mitigation of both intracell and intercell interference using the explicit knowledge of the structure of both types of interference and possibly detecting the data sent by more than one BS.

The organization of the paper envision the description of the system model in Section II, the proposed linear detection schemes in Section III and their typical operating modes in Section IV. A unified sliding window formulation that holds for all proposed linear detectors under any of the considered operation modes is presented in Section V. A theoretical performance analysis is derived in Section VI, while numerical results assessing the receivers performance are presented in Section VII. Finally, conclusions are drawn.

II. System Model

We first focus on a single-cell scenario shown in Fig. 1, where the J synchronous intracell codes are active. We denote the transmitter and receiver filter impulse responses by $p(t)$ and $q(t)$, respectively. Assuming the sampling rate of $W = (\beta)/(T_c)$, where β is the oversampling factor, we choose the receiving filter $q(t)$ to be a low-pass filter whose squared frequency response has vestigial symmetry around frequency $W/2$ [5]. The low mobility environment is modeled by a slowly varying multipath fading channel $h(t)$ and the received signal is further corrupted by $\nu(t)$, an AWGN. The jth OVSF channelization code (Walsh-Hadamard sequence) $(w_j(0), w_j(1), \ldots, w_j(Q_j - 1))$ with spreading factor $Q_j \in \{1, 2, 4, 8, 16\}$ modulates the data sequence $\{a_j(n)\}$ $(j = 1, 2, \ldots, J)$, whose ticking is aligned to the chip sequence by symbol repetition $(\uparrow Q_j)$. The chip interval T_c is constant, while the symbol interval $T_j = Q_j T_c$ may be different from stream to stream. The BS-specific scrambling code, whose length is equal to the maximum possible spreading factor $Q_{\max} = 16$, is described by referring to the jth code symbol interval as follows:

$$z(n;i); \quad n = 0, 1, \ldots, \frac{Q_{\max}}{Q_j} - 1, \quad \text{and} \quad i = 0, 1, \ldots, Q_j - 1 \quad (1)$$

where index n ticks with the symbol intervals of the jth user while index i runs on chip intervals. Finally, we define the structured periodically time-varying spreading code

$$c_j(n;i) \triangleq w_j(i) z(|n-1|_{Q_{\max}/Q_j}; i), \quad n = 1, 2, \ldots \quad \text{and} \quad i = 0, 1, \ldots, Q_j - 1 \quad (2)$$

where "$\triangleq$" means equal by definition, and we have used the operator $|i|_L \triangleq i \bmod L$. The sequence $c_j(n;i)$ and the sequence $z(n;i)$ have the same period equal to $Q_{\max}/Q_j$.

Assuming a linear modulation format, the signal after the front-end filter $q(t)$ has the following complex-valued baseband representation:

$$y(t) = \sum_{j=1}^{J} \sum_{n} a_j(n) \times \sum_{i=0}^{Q_j - 1} c_j(n;i) f(t - (n-1)T_j - iT_c) + v(t) \quad (3)$$

where $f(t)$ is the overall channel impulse response given by the convolution of the chip-shaping pulse $p(t)$ with the multipath channel response $h(t) = \sum_l h_l \delta(t - \tau_l)$ (common to all users). Because of time spread in the chip pulse (the square root raised cosine) and in the channel delay, the overall channel response $f(t)$ exhibits a delay spread equal to P chip intervals, where $P \geq 1$. In defining $h(t)$, we have implicitly assumed that it remains unchanged over the burst duration. The additive noise $v(t)$ is the result of the low pass filtering of $\nu(t)$.

We modify (3) by defining a chip sequence $\{b_j(k)\}$ corresponding to the data sequence $\{a_j(n)\}$ of the jth user $b_j(k) \triangleq a_j(n) c_j(n; |k-1|_{Q_j})$ $(k = 1, 2, \ldots; n = \lceil k/Q_j \rceil$, where $\lceil x \rceil$ denotes the smallest integer equal or greater than $x)$. Equation (3) can be rewritten as

$$y(t) = \sum_{j=1}^{J} \sum_{k} b_j(k) f(t - (k-1)T_c) + v(t). \quad (4)$$

The received signal $y(t)$ is sampled at rate $W = \beta/T_c$. By defining the polyphase representation [17] of a sampled function $g(t)$ by $g_m(i) = g((i\beta - m)/W)$ $(m = 1, 2, \ldots, \beta)$ we have

$$y_m(i) = \sum_{j=1}^{J} \sum_{k=0}^{P-1} f_m(k+1) b_j(i-k) + v_m(i) \quad (5)$$

where the last identity holds since the function $f(t)$ is causal and has a finite support.

We build an observation vector by stacking βN observations $y_m(i)$ (starting at the ith chip interval and spanning N chip intervals backward) as follows:

$$\mathbf{y}^{(N)}(i) \triangleq [y_1(i-N+1), \ldots, y_\beta(i-N+1), \ldots, \times y_1(i), \ldots, y_\beta(i)]^T. \quad (6)$$

A. Single-Cell Discrete-Time Models

In order to express (6) in terms of the channel samples, spreading codes and data, we define the $\beta N \times (P+N-1)$-dimensional matrix

$$\mathbf{F}^{(N)} \triangleq \begin{bmatrix} \mathbf{f}(P-1) & \cdots & \mathbf{f}(0) & & 0 \\ & \ddots & & \ddots & \\ 0 & & \mathbf{f}(P-1) & \cdots & \mathbf{f}(0) \end{bmatrix} \quad (7)$$

where $\mathbf{f}(k) = [f_1(k+1), \ldots, f_\beta(k+1)]^T$. By denoting $n_j \triangleq \lceil (P+N+Q_j-2)/(Q_j) \rceil$, and introducing the symbol-rate ticking index $n(i) \triangleq \lceil i/Q_j \rceil$, we define the matrix as shown in (8) at the bottom of the page, whose dimension is $(P+N-1) \times n_j$. The following n_j-dimensional data string

$$\mathbf{a}_j^{(N)}(i) \triangleq [a_j(n(i)-n_j+1), \ldots, a_j(n(i)-l_j+1), \ldots, \times a_j(n(i))]^T \quad (9)$$

accounts for the maximum length of the jth user-specific involved sequence in the observation $\mathbf{y}^{(N)}(i)$. The parameter $l_j \triangleq \lceil (P+Q_j-1)/(Q_j) \rceil$ highlighted in (8) and (9) accounts for the maximum span of ISI that affects each scalar observation ($l_j = n_j$ when $N = 1$). Let us observe that the ISI span is larger for a smaller spreading factor and vice versa. By defining, in analogy with (6), the βN-dimensional vector of white noise samples $\mathbf{v}^{(N)}(i)$, we can write

$$\mathbf{y}^{(N)}(i) = \sum_{j=1}^{J} \mathbf{F}^{(N)} \mathbf{C}_j^{(N)}(i) \mathbf{a}_j^{(N)}(i) + \mathbf{v}^{(N)}(i). \quad (10)$$

We now define $n_t \triangleq \sum_{j=1}^{J} n_j$, which is the total number of symbols of all users who contributes to the observation vector. Moreover, we define the $(P+N-1) \times n_t$-dimensional matrix and the n_t-dimensional vector

$$\mathbf{C}^{(N)}(i) \triangleq \left[\mathbf{C}_1^{(N)}(i), \mathbf{C}_2^{(N)}(i), \ldots, \mathbf{C}_J^{(N)}(i) \right] \quad (11)$$

$$\mathbf{a}^{(N)}(i) \triangleq \left[\mathbf{a}_1^{(N)^T}(i), \mathbf{a}_2^{(N)^T}(i), \ldots, \mathbf{a}_J^{(N)^T}(i) \right]^T \quad (12)$$

which allows us to rewrite (10) as [5]

$$\mathbf{y}^{(N)}(i) = \mathbf{F}^{(N)} \mathbf{C}^{(N)}(i) \mathbf{a}^{(N)}(i) + \mathbf{v}^{(N)}(i). \quad (13)$$

From the definitions of the $(N+P-1)$-dimensional vector $\mathbf{b}^{(N)}(i) \triangleq \mathbf{C}^{(N)}(i)\mathbf{a}^{(N)}(i)$, and the $(\beta N \times n_t)$-dimensional matrix $\mathbf{G}^{(N)}(i) \triangleq \mathbf{F}^{(N)}\mathbf{C}^{(N)}(i)$, we can derive two other useful expressions for the observation vector

$$\mathbf{y}^{(N)}(i) = \mathbf{F}^{(N)} \mathbf{b}^{(N)}(i) + \mathbf{v}^{(N)}(i) \quad (14)$$

$$= \mathbf{G}^{(N)}(i) \mathbf{a}^{(N)}(i) + \mathbf{v}^{(N)}(i). \quad (15)$$

We can reduce the description accuracy of models (10)–(12) by grouping the active intracell codes in two sets: the codes whose contribution to the observation is described in a structured way belong to a set denoted by $\mathcal{S}$; the complementary set $\bar{\mathcal{S}}$ ($|\mathcal{S} \cup \bar{\mathcal{S}}| = J$, where $|\cdot|$ denotes the cardinality of a set) contains the codes whose interference is modeled as colored Gaussian noise, denoted by $\mathbf{z}^{(N)}(i)$. We then define a new global Gaussian colored noise term $\mathbf{n}^{(N)}(i) = \mathbf{z}^{(N)}(i) + \mathbf{v}^{(N)}(i)$, with correlation matrix $\mathbf{R}_{\mathbf{n}}^{(N)}(i) = \sigma_{\mathbf{v}}^2 \mathbf{I}_N + \mathbf{R}_{\mathbf{z}}^{(N)}(i)$, which allows to rewrite (10)–(12) as follows:

$$\mathbf{y}^{(N)}(i) = \mathbf{F}^{(N)} \mathbf{C}^{(N)}(i) \mathbf{a}^{(N)}(i) + \mathbf{n}^{(N)}(i) \quad (16)$$

$$= \mathbf{F}^{(N)} \mathbf{b}^{(N)}(i) + \mathbf{n}^{(N)}(i) \quad (17)$$

$$= \mathbf{G}^{(N)}(i) \mathbf{a}^{(N)}(i) + \mathbf{n}^{(N)}(i). \quad (18)$$

The structured part of (16)–(18) requires a redefinition of $n_t \triangleq \sum_{j \in \mathcal{S}} n_j$. Matrix $\mathbf{F}^{(N)}$ is still given by (7), while matrix $\mathbf{C}^{(N)}(i)$ and vector $\mathbf{a}^{(N)}(i)$ are obtained by puncturing (11) and (12) with the rule "$j \notin \mathcal{S}$". The relationships $\mathbf{b}^{(N)}(i) = \mathbf{C}^{(N)}(i)\mathbf{a}^{(N)}(i)$ and $\mathbf{G}^{(N)}(i) = \mathbf{F}^{(N)}\mathbf{C}^{(N)}(i)$ remain formally unchanged.

B. Multiple Cell Discrete-Time Model

In a multiple cell scenario shown in Fig. 2, the most general structured expressions for vector (6) is given by

$$\mathbf{y}^{(N)}(i) = \sum_{j=1}^{J_d} \mathbf{F}_d^{(N)} \mathbf{C}_{j,d}^{(N)}(i) \mathbf{a}_{j,d}^{(N)}(i) + \sum_{\lambda=1}^{L} \sum_{j=1}^{J_\lambda} \mathbf{F}_\lambda^{(N)} \mathbf{C}_{j,\lambda}^{(N)}(i) \mathbf{a}_{j,\lambda}^{(N)}(i) + \mathbf{v}^{(N)}(i) \quad (19)$$

$$= \sum_{j=1}^{J_d} \mathbf{F}^{(N)} \mathbf{b}_{j,d}^{(N)}(i) + \sum_{\lambda=1}^{L} \sum_{j=1}^{J_\lambda} \mathbf{F}_\lambda^{(N)} \mathbf{b}_{j,\lambda}^{(N)}(i) + \mathbf{v}^{(N)}(i) \quad (20)$$

$$\mathbf{C}_j^{(N)}(i) \triangleq \begin{bmatrix} c_j(n(i)-n_j+1; |i-N-P+1|_{Q_j}) & & & & 0 \\ \vdots & & & & \\ c_j(n(i)-n_j+1; Q_j-1) & & & & \\ & \ddots & & & \\ & & c_j(n(i)-l_j+1;0) & & \\ & & \vdots & & \\ & & c_j(n(i)-l_j+1; Q_j-1) & & \\ & & & \ddots & \\ & & & & c_j(n(i);0) \\ & & & & \vdots \\ 0 & & & & c_j(n(i); |i-1|_{Q_j}) \end{bmatrix} \quad (8)$$

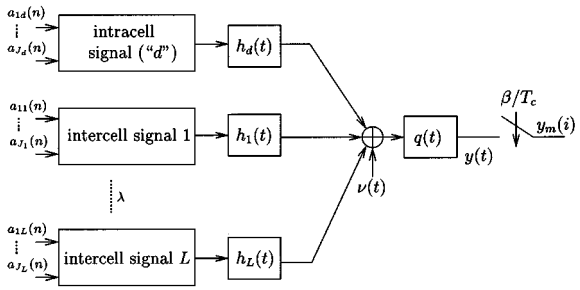

Fig. 2. Model of the considered multiple cell system.

$$= \sum_{j=1}^{J_d} \mathbf{G}_{j,d}^{(N)}(i)\mathbf{a}_{j,d}^{(N)}(i) + \sum_{\lambda=1}^{L}\sum_{j=1}^{J_\lambda} \mathbf{G}_{j,\lambda}^{(N)}(i)\mathbf{a}_{j,\lambda}^{(N)}(i) + \mathbf{v}^{(N)}(i) \quad (21)$$

where we identify with subscript "d" the desired intracell signal. The summation over λ accounts for L beams of block-synchronous intercell signals. J_d and J_λ are the number of active codes in the desired cell and in the λth interfering cell, respectively. Expressions (19)–(21) can be simplified in terms of notation, according to different level of complexity in the description of the interference. In accordance with [4], we introduce two multiple-cell models, which both assume a complete structured description ($|\mathcal{S}| = J_d$) of the intracell signal.

The first model deploys a purely statistical description of the intercell interference which allows to reformulate (19)–(21) as

$$\mathbf{y}^{(N)}(i) = \mathbf{F}_d^{(N)}\mathbf{C}_d^{(N)}(i)\mathbf{a}_d^{(N)}(i) + \mathbf{n}^{(N)}(i) \quad (22)$$

$$= \mathbf{F}_d^{(N)}\mathbf{b}_d^{(N)}(i) + \mathbf{n}^{(N)}(i) \quad (23)$$

$$= \mathbf{G}_d^{(N)}(i)\mathbf{a}_d^{(N)}(i) + \mathbf{n}^{(N)}(i) \quad (24)$$

where in this case, the overall noise term $\mathbf{n}^{(N)}(i) \triangleq \mathbf{v}^{(N)}(i) + \mathbf{z}^{(N)}(i)$, with correlation matrix $\mathbf{R}_{\mathbf{n}}^{(N)}(i) = \sigma_{\mathbf{v}}^2\mathbf{I}_N + \mathbf{R}_{\mathbf{z}}^{(N)}(i)$ includes thermal noise $\mathbf{v}^{(N)}(i)$ and intercell interference $\mathbf{z}^{(N)}(i)$.

The second model [4] is useful when we have knowledge of all interference parameters allowing for a fully structured interference mitigation. Recalling that intercell interferers have the same structure of the intracell signal, we can rewrite (19)–(21) as

$$\mathbf{y}^{(N)}(i) = \mathbf{F}_d^{(N)}\mathbf{C}_d^{(N)}(i)\mathbf{a}_d^{(N)}(i) + \sum_{\lambda=1}^{L}\mathbf{F}_\lambda^{(N)}\mathbf{C}_\lambda^{(N)}(i)\mathbf{a}_\lambda^{(N)}(i) + \mathbf{v}^{(N)}(i) \quad (25)$$

$$= \mathbf{F}_d^{(N)}\mathbf{b}_d^{(N)}(i) + \sum_{\lambda=1}^{L}\mathbf{F}_\lambda^{(N)}\mathbf{b}_\lambda^{(N)}(i) + \mathbf{v}^{(N)}(i) \quad (26)$$

$$= \mathbf{G}_d^{(N)}(i)\mathbf{a}_d^{(N)}(i) + \sum_{\lambda=1}^{L}\mathbf{G}_\lambda^{(N)}(i)\mathbf{a}_\lambda^{(N)}(i) + \mathbf{v}^{(N)}(i) \quad (27)$$

where in the definition of $\mathbf{C}_\lambda^{(N)}(i)$ and $\mathbf{a}_\lambda^{(N)}(i)$ we have assumed $|\mathcal{S}_\lambda| = J_\lambda$.

The link between observation models (25)–(27) and (22)–(24) is given by the following:

$$\mathbf{z}^{(N)}(i) = \sum_{\lambda=1}^{L}\mathbf{F}_\lambda^{(N)}\mathbf{b}_\lambda^{(N)}(i) = \sum_{\lambda=1}^{L}\mathbf{F}_\lambda^{(N)}\mathbf{C}_\lambda^{(N)}(i)\mathbf{a}_\lambda^{(N)}(i) = \sum_{\lambda=1}^{L}\mathbf{G}_\lambda^{(N)}(i)\mathbf{a}_\lambda^{(N)}(i). \quad (28)$$

By using the definitions of [4] (see (29)–(34) at the bottom of the page), we can express the observation in the following extremely compact notation:

$$\mathbf{y}^{(N)}(i) = \mathbf{F}^{(N)}\mathbf{b}^{(N)}(i) + \mathbf{v}^{(N)}(i) \quad (35)$$

$$= \mathbf{F}^{(N)}\mathbf{C}^{(N)}(i)\mathbf{a}^{(N)}(i) + \mathbf{v}^{(N)}(i) \quad (36)$$

$$= \mathbf{G}^{(N)}(i)\mathbf{a}^{(N)}(i) + \mathbf{v}^{(N)}(i) \quad (37)$$

where $\mathbf{F}^{(N)}, \mathbf{b}^{(N)}(i), \mathbf{a}^{(N)}(i), \mathbf{C}^{(N)}(i)$, and $\mathbf{G}^{(N)}(i)$ take into account the parameters of all the interfering cells including the desired one. This model describes, in a compact but structured notation, both the desired intracell signal and the intercell interference.

III. Proposed Linear Detectors

In this section, we present four types of linear detectors that operate assuming that all the parameters (spreading codes,

$$n_t \triangleq \left(n_{t,d} + \sum_{\lambda=1}^{L} n_{t_\lambda}\right) \quad (29)$$

$$\mathbf{F}^{(N)} \triangleq \left[\mathbf{F}_d^{(N)}, \mathbf{F}_1^{(N)}, \ldots, \mathbf{F}_L^{(N)}\right], \quad \beta N \times (L+1)(P+N-1) \quad (30)$$

$$\mathbf{b}^{(N)}(i) \triangleq \left[\mathbf{b}_d^T(i), \mathbf{b}_1^T(i), \ldots, \mathbf{b}_L^T(i)\right]^T, \quad (L+1)(N+P-1) \times 1 \quad (31)$$

$$\mathbf{a}^{(N)}(i) \triangleq \left[\mathbf{a}_d^{(N)\,T}(i), \mathbf{a}_1^{(N)\,T}(i), \ldots, \mathbf{a}_L^{(N)\,T}(i)\right]^T, \quad n_t \times 1 \quad (32)$$

$$\mathbf{C}^{(N)}(i) \triangleq \operatorname{diag}\left[\mathbf{C}_d^{(N)}(i), \mathbf{C}_1^{(N)}(i), \ldots, \mathbf{C}_L^{(N)}(i)\right], \quad (L+1)(P+N-1) \times n_t \quad (33)$$

$$\mathbf{G}^{(N)}(i) \triangleq \left[\mathbf{G}_d^{(N)}(i), \mathbf{G}_1^{(N)}(i), \ldots, \mathbf{G}_L^{(N)}(i)\right], \quad \beta N \times n_t \quad (34)$$

channel coefficients) in the "structured" part of the observation $\mathbf{y}^{(N)}(i)$ are known or estimated, and the "unstructured" part of the observation (noise in a wide sense) has a known or estimated correlation matrix. The task of the detectors is as follows: given the observation vector $\mathbf{y}^{(N)}(i)$, expressed by any of the single-cell models or multiple-cell models find the best (according to some criterion) linear detector that detects all the data on which $\mathbf{y}^{(N)}(i)$ depends. In order to simplify the notation, we drop the superscript $^{(N)}$ in all vectors and matrices, in the rest of this section. Two types of interference arise in the system under consideration: ISI and MAI due to the deployment of oversampling and due to the presence of multipath propagation. ISI can be alleviated by equalization, and MAI, by interference mitigation, which can be realized jointly or separately using channel estimates obtained from the midamble.

In two of the proposed multiuser detectors, we counteract both MAI and ISI simultaneously utilizing the ZF or MMSE criterion applied on observation models (15), (18), (24), or (37) which describes the structured part observation as a linear transformation of the data vector operated by a matrix $\mathbf{G}(i)$. Through a linear transformation described by a properly defined matrix $\mathbf{T}_{\mathbf{a}}(i)$ (an $n_t \times \beta N$ matrix), we obtain an n_t-dimensional vector of soft decision $\mathbf{x}_{\mathbf{a}}(i)$ for the transmitted data $\mathbf{a}(i)$

$$\mathbf{x}_{\mathbf{a}}(i) = \mathbf{T}_{\mathbf{a}}(i)\mathbf{y}(i). \tag{38}$$

Two other schemes are designed to operate with observation models (14), (17), (23), or (35) which describes the structured part observation as a linear transformation of the modulated chip vector operated by a matrix $\mathbf{F}$. These schemes use the ZF or MMSE criterion to mitigate only ISI in order to reduce the complexity. Using a different transformation $\mathbf{T}_{\mathbf{b}}(i)$ (a $(P+N-1)\times\beta N$ matrix), these detectors attempt to restore the orthogonality of the codes, by constructing an $(N+P-1)$-dimensional vector of soft decision $\mathbf{x}_{\mathbf{b}}(i)$ for the chip sequence $\mathbf{b}(i)$

$$\mathbf{x}_{\mathbf{b}}(i) = \mathbf{T}_{\mathbf{b}}(i)\mathbf{y}(i). \tag{39}$$

Then, an additional linear transformation is required to mitigate the MAI. This step is a conventional detection scheme that uses the code matrix $\mathbf{C}(i)$

$$\mathbf{x}_{\mathbf{a}}(i) = \mathbf{C}^H(i)\mathbf{x}_{\mathbf{b}}(i) \tag{40}$$

where ^{H} means "transposition and complex conjugation." The transformation (40) relies on the fact that

$$\mathbf{C}^H(i)\mathbf{C}(i) = \mathbf{I}_{n_t} \tag{41}$$

due to the orthogonality of the Walsh-Hadamard codes. Note that (41) does not strictly hold except when the detection window includes all useful samples of each data block shown in Fig. 4, i.e., its length is $N = M + P - 1$ where M is the number of chip intervals in a data block. Otherwise, there are boundary effects, predictable from the structure of $\mathbf{C}(i)$, which introduce residual MAI into the decision variables for "peripheric" symbols of each user. In fact, the symbol interval of a peripheric symbol is only partially included by the observation window. These symbols are excluded from the sliding window detection algorithm described in Section V.

Eventually, a symbol by symbol decision device produces hard decisions for the transmitted data

$$\hat{\mathbf{a}}(i) = \mathrm{quant}[\mathbf{x}_{\mathbf{a}}(i)]. \tag{42}$$

In the following section, we present the general version of the four detection algorithms, which are formulated as if the data of all active codes must be detected. If this is not the case, the linear transformation can be redefined for an appropriate subspace, i.e., only the relevant FIR filters of the desired codes (appropriate rows of the matrix $\mathbf{T}(i)$ that describes the linear detector) need to be used. All the detection schemes presented below require the Cholesky decomposition $\mathbf{R}_{\mathbf{n}}(i) = \mathbf{L}(i)\mathbf{L}^H(i)$ of the noise covariance matrix.

A. The ZF Detector for Both MAI and ISI (ZF-MI)

It is well known that the ZF detector task is to perform the following minimization [10]:

$$\mathbf{x}_{\mathbf{a},\text{ZF-MI}}(i) = \arg\min_{\mathbf{x}(i)} \|\mathbf{L}^{-1}(i)(\mathbf{y}(i) - \mathbf{G}(i)\mathbf{x}(i))\|^2 \tag{43}$$

whose solution can be casted in problem (38), if interpreted as a projection problem. Equation (43) is solved by the linear transformation

$$\mathbf{T}_{\text{ZF-MI}}(i) = [\mathbf{L}^{-1}(i)\mathbf{G}(i)]^{\#}\mathbf{L}^{-1}(i) \tag{44}$$

where $^{\#}$ denotes the pseudo inverse of a matrix. It is easy to show that in this case

$$\begin{aligned}\mathbf{x}_{\mathbf{a},\text{ZF-MI}}(i) &= [\mathbf{L}^{-1}(i)\mathbf{G}(i)]^{\#}\mathbf{L}^{-1}(i)\mathbf{y}(i)\\ &= \mathbf{a}(i) + \mathbf{u}_{\text{ZF-MI}}(i)\end{aligned} \tag{45}$$

where $\mathbf{u}_{\text{ZF-MI}}(i) \triangleq [\mathbf{L}^{-1}(i)\mathbf{G}(i)]^{\#}\mathbf{L}^{-1}(i)\mathbf{n}(i)$ is a new noise process.

Note that due to the constraint $\beta N \geq n_t$, the minimum number of samples to be processed for the feasibility of this detector may be large.

B. The ZF Detector for ISI Only (ZF-I)

A preliminary $(N+P-1)$-dimensional vector $\mathbf{x}_{b,\text{ZF-I}}(i)$ for soft decision can be obtained from the following minimization:

$$\mathbf{x}_{\mathbf{b},\text{ZF-I}}(i) = \arg\min_{\mathbf{x}'(i)} \|\mathbf{L}^{-1}(i)(\mathbf{y}(i) - \mathbf{F}(i)\mathbf{x}'(i))\|^2 \tag{46}$$

whose solution can be interpreted according to (39) as a linear transformation of $\mathbf{y}(i)$ described by

$$\mathbf{T}_{\text{ZF-I}}(i) = [\mathbf{L}^{-1}(i)\mathbf{F}]^{\#}\mathbf{L}^{-1}(i). \tag{47}$$

From the linear estimation theory it is easy to show that

$$\mathbf{x}_{\mathbf{b},\text{ZF-I}}(i) = \mathbf{b}(i) + \mathbf{u}'_{\text{ZF-I}}(i) \tag{48}$$

where $\mathbf{u}'_{\text{ZF-I}}(i) \triangleq [\mathbf{L}^{-1}(i)\mathbf{F}]^{\#}\mathbf{L}^{-1}(i)\mathbf{n}(i)$ is a new noise process.

Then conventional matched filtering described by (40) is required to derive the final n_t-dimensional decision variable $\mathbf{x}_{\mathbf{a},\text{ZF-I}}(i)$ given by

$$\mathbf{x}_{\mathbf{a},\text{ZF-I}}(i) = \mathbf{C}^H(i)\mathbf{x}_{\mathbf{b},\text{ZF-I}}(i) = \mathbf{a}(i) + \mathbf{u}_{\text{ZF-I}}(i) \tag{49}$$

where $\mathbf{u}_{\text{ZF-I}}(i) \triangleq \mathbf{C}^H(i)\mathbf{u}'_{\text{ZF-I}}(i)$ and we used (41).

Note that the constraint $\beta N \geq N + P - 1$ is in general less demanding than that of the previous detector.

C. The MMSE Detector for Mitigation of Both MAI and ISI (MMSE-MI)

The MMSE detector performs the following minimization

$$\mathbf{T}_{\text{MMSE-MI}}(i) = \arg\min_{\mathbf{T}(i)} E_{\mathbf{a}(i),\mathbf{v}(i)} \left[\|\mathbf{a}(i) - \mathbf{T}(i)\mathbf{y}(i)\|^2\right] \tag{50}$$

such that the n_t-dimensional vector of soft decisions $\mathbf{x}_{\mathbf{a},\text{MMSE-MI}}(i) \triangleq \mathbf{T}_{\text{MMSE-MI}}(i)\mathbf{y}(i)$ is the best solution (in the minimum mean square sense) to the problem of predicting $\mathbf{a}(i)$, regarded as continuous variables.

The solution to this problem leads to the linear transformation described by

$$\begin{aligned}&\mathbf{T}_{\text{MMSE-MI}}(i)\\ &\quad = E[\mathbf{a}(i)\mathbf{y}^H(i)]\{E[\mathbf{y}(i)\mathbf{y}^H(i)]\}^{-1}\\ &\quad = \left[\mathbf{G}^H(i)\mathbf{R}_{\mathbf{n}}^{-1}(i)\mathbf{G}(i) + \mathbf{R}_{\mathbf{a}}^{-1}(i)\right]^{-1}\mathbf{G}^H(i)\mathbf{R}_{\mathbf{n}}^{-1}(i)\end{aligned} \tag{51}$$

where $\mathbf{R}_{\mathbf{a}}(i) = E[\mathbf{a}(i)\mathbf{a}^H(i)]$. It can be shown that [10]

$$\begin{aligned}&\mathbf{x}_{\mathbf{a},\text{MMSE-MI}}(i)\\ &\quad = \left[\mathbf{I}_{n_t} + (\mathbf{R}_{\mathbf{a}}(i)\mathbf{G}^H(i)\mathbf{R}_{\mathbf{n}}^{-1}(i)\mathbf{G}(i))^{-1}\right]^{-1}\mathbf{x}_{\mathbf{a},\text{ZF-MI}}(i)\\ &\quad \triangleq \mathbf{W}_{\text{MI}}(i)\mathbf{x}_{\mathbf{a},\text{ZF-MI}}(i)\end{aligned} \tag{52}$$

where the $n_t \times n_t$ square matrix $\mathbf{W}_{\text{MI}}(i)$ is a Wiener estimator, which observes $\mathbf{x}_{\mathbf{a},\text{ZF-MI}}(i)$ and produces the MMSE soft estimate $\mathbf{x}_{\mathbf{a},\text{MMSE-MI}}(i)$ of $\mathbf{a}(i)$, reducing the performance degradation of the ZF detector, whose decisions do not take into account the noise correlations among the decision variables [10].

Note that this time there are no constraints on the minimum size of the observation vector $\mathbf{y}(i)$.

D. The MMSE Detector for Mitigation of ISI Only (MMSE-I)

The detector realizes the following minimization:

$$\mathbf{T}_{\text{MMSE-I}}(i) = \arg\min_{\mathbf{T}(i)} E_{\mathbf{b}(i),\mathbf{v}(i)}[\|\mathbf{b}(i) - \mathbf{T}(i)\mathbf{y}(i)\|^2] \tag{53}$$

which is solved by the linear transformation described by the $(N+P-1)\times \beta N$-dimensional matrix

$$\mathbf{T}_{\text{MMSE-I}}(i) = \left[\mathbf{F}^H\mathbf{R}_{\mathbf{n}}^{-1}(i)\mathbf{F} + \mathbf{R}_{\mathbf{b}}^{-1}(i)\right]^{-1}\mathbf{F}^H\mathbf{R}_{\mathbf{n}}^{-1}(i) \tag{54}$$

where $\mathbf{R}_{\mathbf{b}}(i) = E[\mathbf{b}(i)\mathbf{b}^H(i)] = \mathbf{C}(i)\mathbf{R}_{\mathbf{a}}(i)\mathbf{C}^H(i)$. Soft decisions are given by

$$\begin{aligned}&\mathbf{x}_{\mathbf{b},\text{MMSE-I}}(i)\\ &\quad = \left[\mathbf{I}_{N+P-1} + (\mathbf{R}_{\mathbf{b}}(i)\mathbf{F}^H\mathbf{R}_{\mathbf{n}}^{-1}(i)\mathbf{F})^{-1}\right]^{-1}\mathbf{x}_{\mathbf{b},\text{ZF-I}}(i)\\ &\quad \triangleq \mathbf{W}_I(i)\mathbf{x}_{\mathbf{b},\text{ZF-I}}(i) = \mathbf{W}_I(i)\mathbf{b}(i) + \mathbf{u}'_{\text{MMSE-I}}(i)\end{aligned} \tag{55}$$

where the $(N+P-1)\times(N+P-1)$ square matrix $\mathbf{W}_I(i)$ is a Wiener estimator, which observes $\mathbf{x}_{\mathbf{b},\text{ZF-I}}(i)$ and produces the MMSE soft estimate $\mathbf{x}_{\mathbf{b},\text{MMSE-I}}(i)$ of $\mathbf{b}(i)$ and $\mathbf{u}'_{\text{MMSE-I}}(i) = \mathbf{W}_I(i)\mathbf{u}'_{\text{ZF-I}}(i)$ is a new noise process.

We can now use a time-discrete matched filter to the users' (structured) codes $\mathbf{C}^H(i)$, whose n_t-dimensional output $\mathbf{x}_{\mathbf{a},\text{MMSE-I}}(i)$ is a soft estimate of $\mathbf{a}(i)$, given by

$$\begin{aligned}\mathbf{x}_{\mathbf{a},\text{MMSE-I}}(i) &= \mathbf{C}^H(i)\mathbf{x}_{\mathbf{b},\text{MMSE-I}}(i)\\ &= \mathbf{C}^H(i)\mathbf{W}_I(i)\mathbf{b}(i) + \mathbf{u}_{\text{MMSE-I}}(i)\end{aligned} \tag{56}$$

where $\mathbf{u}_{\text{MMSE-I}}(i) \triangleq \mathbf{C}^H(i)\mathbf{u}'_{\text{MMSE-I}}(i)$. Note that in (56) a residual MAI and ISI is present in all decision variables.

Also in this case, there are no constraints on the size of the observation vector $\mathbf{y}(i)$.

IV. Typical Operating Modes of the Proposed Linear Detectors

The direct intracell interference mitigation feature is always set "on" while the intercell interference is treated differently according to some criteria, for example its power level $\sigma_{\mathbf{z}}^2$ compared to the whole signal power $\sigma_{\mathbf{y}}^2$.

Some examples of the operating modes are identified and described in the following list.

1) **Structured Intracell Interference Mitigation**: This is the case of a single cell situation in a strict ($\sigma_{\mathbf{z}}^2 = 0$) or approximate sense ($\sigma_{\mathbf{z}}^2 \ll \sigma_{\mathbf{y}}^2$), for which the observation models (13)–(15) apply. The data part of the observation is completely structured ($|\mathcal{S}| = J_d$) and the receiver realizes a standard intracell interference mitigation as thoroughly described in [5].
2) **Unstructured Intracell Interference Mitigation**: This strategy is again used in a single cell scenario ($\sigma_{\mathbf{z}}^2 = 0$ or $\sigma_{\mathbf{z}}^2 \ll \sigma_{\mathbf{y}}^2$), and it deploys a statistical description of the intracell codes, which are not of interest of the considered MS (set S). This interference is modeled as colored Gaussian noise whose covariance matrix is evaluated in closed form (as shown in Appendix II). The observation models (16)–(18) apply in this case.
3) **Structured Intracell and Unstructured Intercell Interference Mitigation**: This strategy can be adopted when the intercell interference power $\sigma_{\mathbf{z}}^2$ is not negligible. In this case the observation models (22)–(24) are used, and the global noise term $\mathbf{n}(i)$ is modeled as colored Gaussian noise whose covariance matrix $\mathbf{R}_{\mathbf{n}}$ is either estimated or evaluated in closed form.
4) **Structured Intracell and Intercell Interference Mitigation**: This strategy is typical of the soft hand-over procedure. The observation model is given by the block-synchronous observation (35)–(37). The receiver acts as a structured multicell direct interference suppressor of both the interference coming from the original cell and that coming from the hand-over candidate cell(s), with the capability of detecting both the data of the desired and interfering cell.

V. Sliding Window Formulation

The detectors presented in the previous section are block detectors. Finite complexity formulations of these detectors are necessary in order to employ them in practical receivers. The following derivation is referred the linear detector MMSE-MI

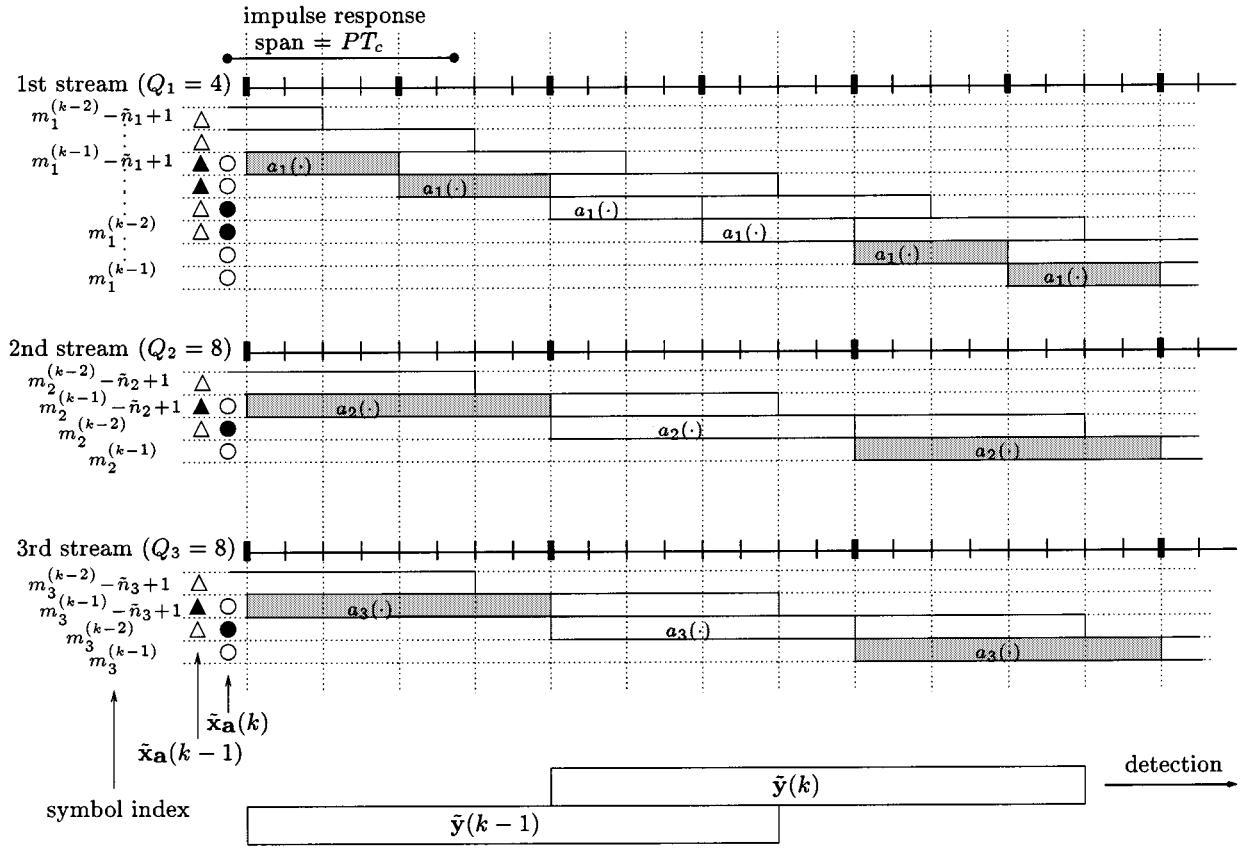

Fig. 3. Example of linear interference mitigation and symbol by symbol detection of a data block with three data streams with different data rates (thick lines separate symbol intervals, thin lines separate chips). In this case, the maximum spreading factor is $Q = 8$. The figures shows the nominal symbol interval (shaded) along with the ISI caused by each symbol. Potential decision variables obtained with the $(k-1)$th and kth observation block denoted by $\tilde{\mathbf{x}}_{\mathbf{a}}(k-1)$ and $\tilde{\mathbf{x}}_{\mathbf{a}}(k)$ are marked with triangles ($\triangle$) and with circles ($\circ$), respectively, and those actually used at each detection step are filled in black. The empty triangles and circles denotes the "peripheric" symbols excluded by the sliding window algorithm. In Table I we provide the numbering of the symbols with reference to those marked with circles.

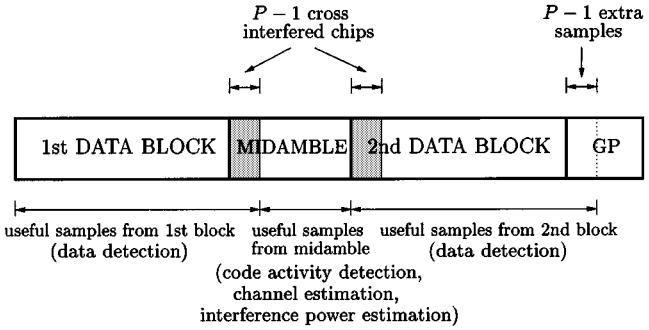

Fig. 4. Format of a physical channel in a TDD time-slot. It consists of two data blocks with a midamble in between. A silent guard period (GP) terminates the data burst.

presented in Section III-C and is demonstrated, for the sake of simplicity, on a single cell environment but it holds for all other types of linear detectors presented in this paper. Detectors that mitigate only ISI can be also used according to this sliding window architecture since the "peripheric" decision variables are properly handled by this algorithm.

The guiding principle for the sliding window formulation is that the block minimization accomplished by the linear detector can be simplified, because the vector $\mathbf{y}^{(N)}(i)$ has stationary statistics if $N \geq Q$, where Q is the maximum spreading factor currently used by the system. The observation window size is set to $\tilde{N} \triangleq (Q+P-1)$ chip intervals, because this size allows to collect all samples that carry useful energy for detection of one symbol of the slowest stream. As a consequence $\tilde{n}_t \triangleq \sum_j \tilde{n}_j$ where $\tilde{n}_j \triangleq \lceil (2(P-1)+Q_j+Q)/(Q_j) \rceil$. In reference to Fig. 3 we define the parameter $K \triangleq (N)/(Q)$ and

$$\tilde{\mathbf{y}}(k) \triangleq \mathbf{y}^{(Q+P-1)}(kQ+P-1) \tag{57}$$

$$\tilde{\mathbf{a}}(k) \triangleq \mathbf{a}^{(Q+P-1)}(kQ+P-1) \tag{58}$$

where $k = 1, 2, \ldots, K$ is an index ticking with the symbol rate of the slowest users. By further defining the matrices

$$\tilde{\mathbf{G}} \triangleq \mathbf{G}^{(Q+P-1)}(kQ+P-1) \tag{59}$$

$$\tilde{\mathbf{R}}_{\mathbf{a}} \triangleq \mathbf{R}_{\mathbf{a}}^{(Q+P-1)}(kQ+P-1) \tag{60}$$

$$\tilde{\mathbf{R}}_{\mathbf{n}} \triangleq \mathbf{R}_{\mathbf{n}}^{(Q+P-1)}(kQ+P-1) \tag{61}$$

$$\tilde{\mathbf{W}}_{\mathrm{MI}} \triangleq \mathbf{W}_{\mathrm{MI}}^{(Q+P-1)}(kQ+P-1) \tag{62}$$

that are all independent of the detection step k, it is easy to show that the $\tilde{n}_t \times \beta(Q+P-1)$-dimensional matrix

$$\begin{aligned}\tilde{\mathbf{T}} &\triangleq \left(\tilde{\mathbf{G}}^H \tilde{\mathbf{R}}_{\mathbf{n}}^{-1} \tilde{\mathbf{G}} + \tilde{\mathbf{R}}_{\mathbf{a}}^{-1}\right)^{-1} \tilde{\mathbf{G}}^H \tilde{\mathbf{R}}_{\mathbf{n}}^{-1} \\ &= \tilde{\mathbf{W}}_{\mathrm{MI}} \left(\tilde{\mathbf{G}}^H \tilde{\mathbf{R}}_{\mathbf{n}}^{-1} \tilde{\mathbf{G}}\right)^{-1} \tilde{\mathbf{G}}^H \tilde{\mathbf{R}}_{\mathbf{n}}^{-1}\end{aligned} \tag{63}$$

TABLE I
SEQUENCE OF THE SYNCHRONIZATION EPOCHS OF THE DETECTION PROCESS

∘	$m_j^{(k)} - \tilde{n}_j$	first DV of k-th observation block
∘	$m_j^{(k-2)}$	last DV of $(k-2)$-th observation block
∘	$\frac{(k-1)Q}{Q_j}$	DETECTION STOPS using DVs of $(k-1)$-th observation block
•	$\frac{(k-1)Q}{Q_j} + 1$	DETECTIONS STARTS using DVs of k-th observation block
•	$m_j^{(k+1)} - \tilde{n}_j$	first DV of $(k+1)$-th observation block
•	$m_j^{(k-1)}$	last DV of $(k-1)$-th observation block
•	$\frac{kQ}{Q_j}$	DETECTION STOPS using the DVs of k-th observation block
∘	$\frac{kQ}{Q_j} + 1$	DETECTION STARTS using the DVs of the $(k+1)$-th observation block
∘	$m_j^{(k+2)} - \tilde{n}_j$	1st DV of $(k+2)$-th observation block
∘	$m_j^{(k)}$	last DV of k-th observation block

is also independent of the detection step k and its rows are FIR filters that will be used throughout the detection process. We can then derive the $\tilde{n}_t$-dimensional vector $\tilde{\mathbf{x}}_{\mathbf{a}}(k)$ as

$$\tilde{\mathbf{x}}_{\mathbf{a}}(k) = \tilde{\mathbf{T}}\tilde{\mathbf{y}}(k) \quad k = 1, 2, \ldots, K. \tag{64}$$

It is worthwhile to expand $\tilde{\mathbf{x}}_a(k)$, soft-estimate of $\tilde{\mathbf{a}}(k)$, as [see (65) at the bottom of the page] where

$$m_j^{(k)} \triangleq \left\lceil \frac{kQ + P - 1}{Q_j} \right\rceil \quad k = 1, 2, \ldots, K \tag{66}$$

is the first symbol for which we get a decision variable for code j at the kth detection step as described in Table I. Detection of all symbols could be accomplished using a symbol by symbol decision device according to the rule $\hat{\tilde{\mathbf{a}}}(k) = \mathrm{quant}[\tilde{\mathbf{x}}_{\mathbf{a}}(k)]$ for $k = 1, 2, \ldots, K$. For the sake of clarity, note that the argument of $\mathbf{y}(\cdot)$ runs over chip intervals while that of $\tilde{\mathbf{y}}(\cdot), \tilde{\mathbf{a}}(\cdot)$ and $\tilde{\mathbf{x}}_{\mathbf{a}}(\cdot)$ runs over the detection step (which ticks at to the symbol rate of the slowest user).

The total number of potential decision variables for all symbols embraced by the processing window $\tilde{\mathbf{y}}(k)$ is $\tilde{n}_t$ (highlighted with circles in Fig. 3). Nevertheless, for a given processing window $\tilde{\mathbf{y}}(k)$, there are code-specific central subvectors (with length Q/Q_j) of $\tilde{\mathbf{x}}_{\mathbf{a}}(k)$, that yield an optimal decision variable for the corresponding symbols (circles filled in black in Fig. 3) of the data stream carried by the jth code. The other symbols (empty circles in Fig. 3) are optimally detected in the following or preceding processing window, (the squares filled in black in Fig. 3, as an example). Fig. 3 shows how the sliding window algorithms proceeds, and in Table I, we list major synchronization points of the detection process for the jth user, providing the numbering of the decision variables (DVs) marked with circles, which are also reported on the left of the Table I. Table I indicates use of the DVs to realize a continuous detection of the data. This design choice will be

$$\begin{aligned}\tilde{\mathbf{x}}_a(k) = \Big[& x_1\left(m_1^{(k-1)} - \tilde{n}_1 + 1\right), x_1\left(m_1^{(k-1)} - \tilde{n}_1 + 2\right), \ldots, x_1\left(m_1^{(k)}\right), \\ & \vdots \qquad\qquad \vdots \qquad\qquad \vdots \\ & x_J\left(m_J^{(k-1)} - \tilde{n}_J + 1\right), x_J\left(m_J^{(k-1)} - \tilde{n}_J + 2\right), \ldots, x_J\left(m_J^{(k)}\right)\Big]\end{aligned} \tag{65}$$

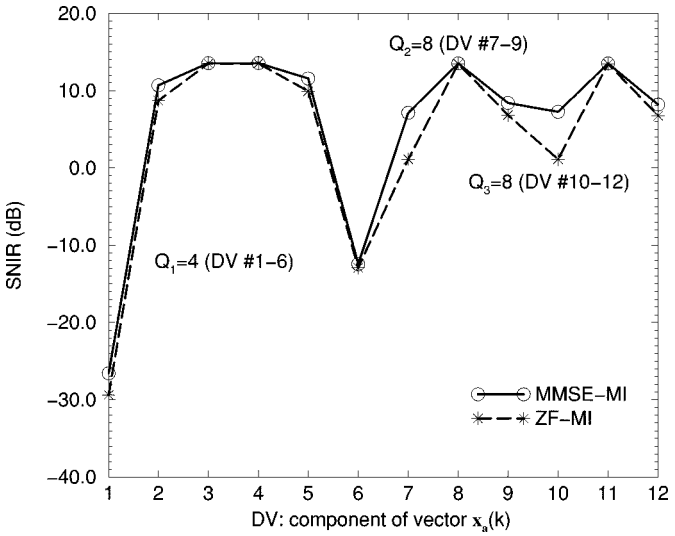

Fig. 5. SNIR as a function of the components (decision variables, DV) of vector $\tilde{\mathbf{x}}_{\mathbf{a}}(k)$ available for a detection scenario with three active codes ($Q_1 = 4, Q_2 = Q_3 = 8$). The symbols with maximum SNIR correspond to the circles filled in black in Fig. 3.

also validated by the results of Fig. 5. The algorithm can be summarized as follows.

- Initialization, once per burst:
  1) based on the information on the active codes and on the estimated value of P, evaluate $\tilde{n}_j \; \forall j \in \mathcal{S}$ and $\tilde{n}_t$.
  2) evaluate transformation matrix $\mathbf{T}$.
  3) for each user j that we want to detect, select the appropriate Q/Q_j rows for the detection of the symbols with maximum signal to noise and interference ratio (SNIR) (filled circles as shown in Table I and Fig. 3).
- Steady state, at each detection step:
  1) use appropriate rows of $\mathbf{T}$ selected in step 3) of the initialization to obtain soft decisions for the users' data;
  2) make a hard decision at each detection step.

As a final remark we also highlight the perfect matching of the proposed sliding window algorithm with the data format of the TDD standard, which is shown in Fig. 4. Two windows, that slides to the right and to the left of the midamble on the range of observation shown are used.

VI. Performance Analysis

A. Exact Bit-Error Probability (BEP) Evaluation

We evaluate the BEP in closed form for the ZF-MI and MMSE-MI (as an example), generalizing, the results of [10], [14] to a multirate system with a simultaneous presence of ISI and MAI.

Using the soft decision vector $\tilde{\mathbf{x}}_{\mathbf{a},\text{ZF-MI}}(\cdot)$ given by (45), we can express the BEP associated to its jth component as

$$P_{e,\text{ZF-MI}}(j) = \mathbf{Q}\left(\sqrt{\frac{E[|a(j)|^2]}{\sigma^2_{u\ \text{ZF-MI}}(j)}}\right), \quad j = 1, 2, \ldots, \tilde{n}_t \tag{67}$$

where $\mathbf{Q}(x)$ is the standard cumulative Gaussian distribution and $\sigma^2_{u\ \text{ZF-MI}}(j) = (\tilde{\mathbf{G}}^H \tilde{\mathbf{R}}_{\mathbf{n}}^{-1} \tilde{\mathbf{G}})^{-1}_{j,j}$, being $(\cdot)_{m,n}$ the operator that returns the element of row m and column n of a matrix.

In the soft decision $\tilde{\mathbf{x}}_{\mathbf{a},\text{MMSE-MI}}(\cdot)$ given by (52), there is a presence of residual ISI and MAI. Hence, in order to evaluate the BEP it is necessary to condition dover all interfering symbols [see (68) at the bottom of the page] where $\mathcal{C}^{\tilde{n}_t}$ denotes the set of all $\tilde{n}_t$-uples whose components are the symbols of the assumed constellation and

$$\sigma^2_{u,\text{MMSE-MI}}(j) = \sigma^2_{u,\text{ZF-MI}}(j) \left(\tilde{\mathbf{W}}_{\text{MI}} \tilde{\mathbf{W}}^H_{\text{MI}}\right)_{j,j}, \quad j = 1, 2, \ldots, \tilde{n}_t. \tag{69}$$

B. Gaussian Approximation for BEP Evaluation

We first express the SNIR as a function of the component j ($j = 1, 2, \ldots, \tilde{n}_t$) of the soft decision vector for both ZF-MI and MMSE-MI detectors

$$\begin{aligned} \mathbf{\Gamma}_{\text{ZF-MI}}(j) &= \frac{E[|a(j)|^2]}{\sigma^2_{u\ \text{ZF-MI}}(j)}, \\ \mathbf{\Gamma}_{\text{MMSE-MI}}(j) &= \frac{|(\tilde{\mathbf{W}}_{\text{MI}})_{j,j}|^2 E[|a(j)|^2]}{\sigma^2_{\text{MAI-ISI}}(j) + \sigma^2_{u\ \text{MMSE-MI}}(j)} \end{aligned} \tag{70}$$

where $\sigma^2_{u,\text{MMSE-MI}}(j)$ is given by (69) and

$$\begin{aligned} \sigma^2_{\text{MAI-ISI}}(j) \triangleq\ & (\tilde{\mathbf{W}}_{\text{MI}} \tilde{\mathbf{R}}_{\mathbf{a}})_{j,j} \\ & - 2\text{Re}\left\{(\tilde{\mathbf{W}}_{\text{MI}} \tilde{\mathbf{R}}_{\mathbf{a}})_{j,j} \left(\tilde{\mathbf{W}}^H_{\text{MI}}\right)_{j,j}\right\} \\ & + E[|a(j)|^2] |(\tilde{\mathbf{W}}_{\text{MI}})_{j,j}|^2. \end{aligned} \tag{71}$$

For the ZF-MI detector, the exact and Gaussian analysis coincide for the ZF-MI detector since noise is given by $\mathbf{u}_{\text{ZF-MI}}$, which is strictly Gaussian. For the MMSE-MI detector, we can use the the Gaussian approximation in the denominator of $\mathbf{\Gamma}_{\text{MMSE-MI}}(j)$, obtaining

$$P_{e\ \text{MMSE-MI}}(j) \approx \mathbf{Q}(\sqrt{\mathbf{\Gamma}_{\text{MMSE-MI}}(j)}) \quad j = 1, 2, \ldots, \tilde{n}_t. \tag{72}$$

As shown in the numerical results, the approximation yields good results even for a low number of active codes, extending the results by Poor and Verdù [14] to multirate systems.

$$P_{e,\text{MMSE-MI}}(j) = \frac{1}{M^{\tilde{n}_t}} \sum_{(a(1),\ldots,a(\tilde{n}_t)) \in \mathcal{C}^{\tilde{n}_t}} \mathbf{Q}\left(\frac{(\tilde{\mathbf{W}}_{\text{MI}})_{j,j} a(j) + \sum_{k=1, k\neq j}^{\tilde{n}_t} (\tilde{\mathbf{W}}_{\text{MI}})_{j,k} a(k)}{\sigma_{u,\text{MMSE-MI}}(j)}\right) \tag{68}$$

VII. Numerical Results

In this section, we present some numerical results to assess the receiver performance. The assumed modulation scheme is binary phase shift keying (BPSK). The chip pulse shaping is a root raised cosine with roll-off $\alpha = 0.22$ and the oversampling factor is $\beta = 2$ with respect to the chip rate equal to 3.840 Mchip/s. The multipath channel is a three-ray channel where the relative power of the three taps are $\sigma^2_{h_0} = 0$ dB, $\sigma^2_{h_1} = -13$ dB, and $\sigma^2_{h_2} = -25$ dB and the delays are $\tau_0 = 0, \tau_1 = 240$ ns, and $\tau_2 = 490$ ns, respectively. The delay spread of the overall channel (convolution of the multipath channel and the chip pulse) is truncated to the value $P = 7$. The OVSF codes have normalized unit energy such that the system operates with constant energy per bit E_b.

We have considered single-cell and two-cell scenarios where the cells are circular with equal radius r. The BSs are located at the center of each cell. For the two-cell scenario we have assumed that the MS can roam within the cell of interest along the line connecting the two BSs. We have also assumed that the power P received by a MS from a BS according to a law $1/D^4$, where D is the distance between the MS and the BS. Defining with P_d and P_i the powers of the two signals received from the serving BS and from the interfering BS, respectively, it is easy to show that at MS we have the following ratio of powers:

$$P_d/P_i = \left(\frac{r+l}{r-l}\right)^4 \tag{73}$$

where l is the distance of the MS from the boundaries of the cell of interest.

A. Multicode Detection Performance

In order to validate the proposed detection strategy, we have plot in Fig. 5 the SNIR expressions given by (70) as functions of $j = 1, 2, \ldots, \tilde{n}_t$. For this purpose we consider a single-cell case with AWGN power of $\sigma^2_{\mathbf{v}} = -10$ dB and three active codes with spreading factors $Q_1 = 4, Q_2 = Q_3 = 8$, the latter being the maximum spreading factor among all the active codes $(Q = 8)$. Accordingly, the processing window has size $\tilde{N} = Q + P - 1 = 14$ and the corresponding components of $\tilde{\mathbf{x}}_{\mathbf{a}}(k)$ given by (64) are $\tilde{n}_t = 12$, where $\tilde{n}_1 = 6$ for the first data stream and $\tilde{n}_2 = \tilde{n}_3 = 3$ for the second and third data streams. Specifically, Fig. 5 presents the SNIR on each of the 12 decision variables for the ZF-MI and the MMSE-MI detectors. Considering the first stream $(Q_1 = 4)$ it can be seen that among the $\tilde{n}_1 = 6$ DVs, # 1, 2, 5, and 6 are affected by a poor SNIR performance. The low SNIR is easily justified by considering that the observation vector $\tilde{\mathbf{y}}(k)$ does not collect all the received energy available for the detection of those symbols. Detection of $(Q)/(Q_1) = 2$ DVs # 3 and # 4 only, which have maximum SNIR, is recommended. A similar choice must be done for the other two data streams with $Q_2 = Q_3 = 8$, where only $(Q)/(Q_2) = (Q)/(Q_3) = 1$ DVs # 8 and # 11 are retained for detection.

B. Single-Cell BEP and BER Performance

In this section, we present a performance evaluation of the proposed receivers in terms of the average BEP, derived by the theoretical analysis (presented in Section VI), or the average bit error rate (BER), obtained by Monte-Carlo simulation. BEP and BER are plotted as a function of E_b/N_0, the average received energy per bit over noise spectral density. All numerical results, except those of Fig. 9, are obtained assuming a perfect channel estimation, hence, the performance curve can be regarded as a lower bound for any practical receiver.

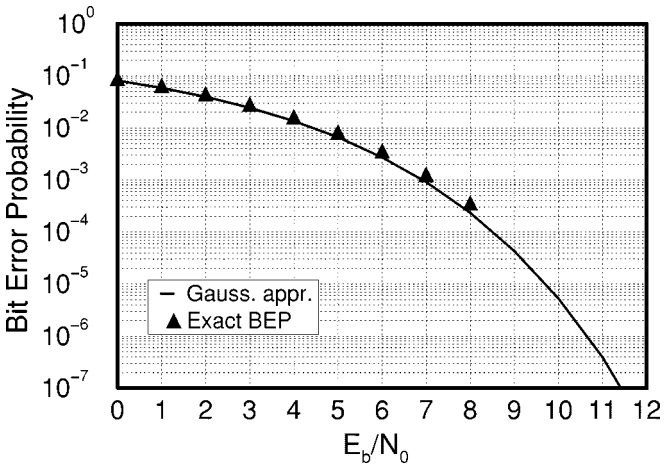

Fig. 6. Comparison between BER performance obtained by the Gaussian approximation and the exact evaluation, for MMSE-MI receiver assuming a deterministic Rice channel, and three active codes: $Q_1 = 4, Q_2 = 8, Q_3 = 16$ [P. Castoldi, "*Multiuser Detection in CDMA Mobile Terminals*," to be published by Artech House, Norwood, MA, May 2002, reprinted with permission].

In Fig. 6, we present a BEP comparison between the approximate analysis based on the Gaussian approximation (solid line) and the exact analysis (points marked with triangles) for a single-cell system with three active codes $Q_1 = 4, Q_2 = 8$, and $Q_3 = 16$. The theoretical analysis based on the Gaussian approximation is in excellent agreement with the exact BEP evaluation, extending the validity of the Gaussian approach, outlined in [14], to multirate systems.

In Fig. 7, we present the BER performance of the four types of receiver operating in a single-cell scenario, where three codes with spreading factor $Q_1 = 4, Q_2 = Q_3 = 8$ are active. The BER performance has been evaluated for the data stream of the fastest user $(Q_1 = 4)$. The detection algorithms have been tested under two extreme situations: (1) a pure Rice channel with deterministic amplitude of the echoes; and (2) a pure Rayleigh fading channel where the echo amplitudes are assumed to be a random variable but remain unchanged along the whole burst. For a deterministic channel (curves marked with circles) no difference in performance can be seen among the ZF-MI, MMSE-MI and MMSE-I and a slight performance degradation is exhibited by the ZF-I receiver. On the contrary, in the presence of a pure Rayleigh channel the performance is significantly worse than the previous one. The ZF-MI, MMSE-MI, and MMSE-I receiver perform approximately the same, equal to the single user bound for a random channel, while the ZF-I performs moderately worse than the others.

In Fig. 8, we present the performance of the ZF-MI and MMSE-MI receivers, for a constant deterministic channel, under various system loads. The normalized system load is defined as $\rho = \sum_i Q_i^{-1}$ where i runs over all active codes $(0 \leq \rho \leq 1)$. The performance is almost independent of the combination of spreading factors used by the system under light

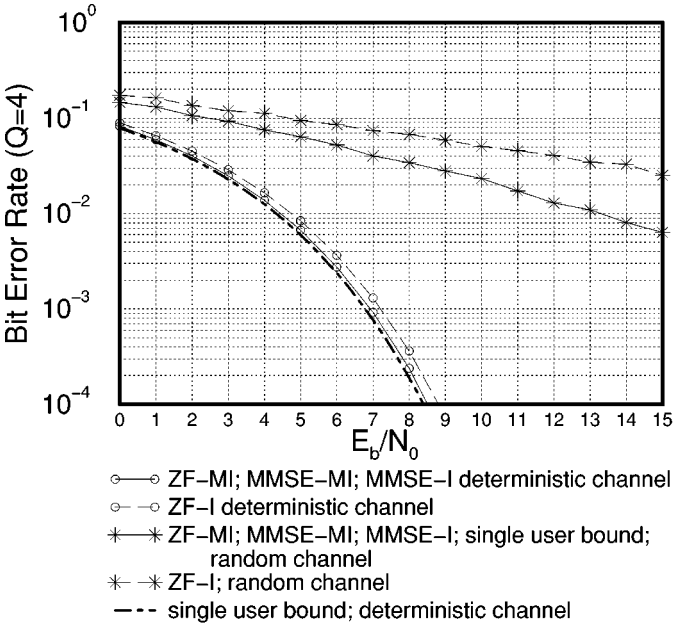

Fig. 7. BER performance of the proposed receivers as a function of E_b/N_0 for a deterministic channel and a random channel.

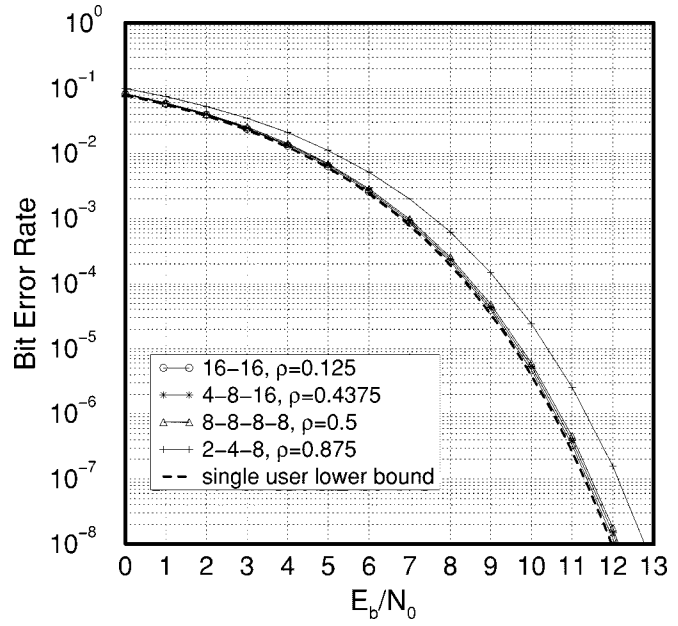

Fig. 8. BER performance of the ZF-MI and MMSE-MI receivers as a function of E_b/N_0, for various system loads ρ.

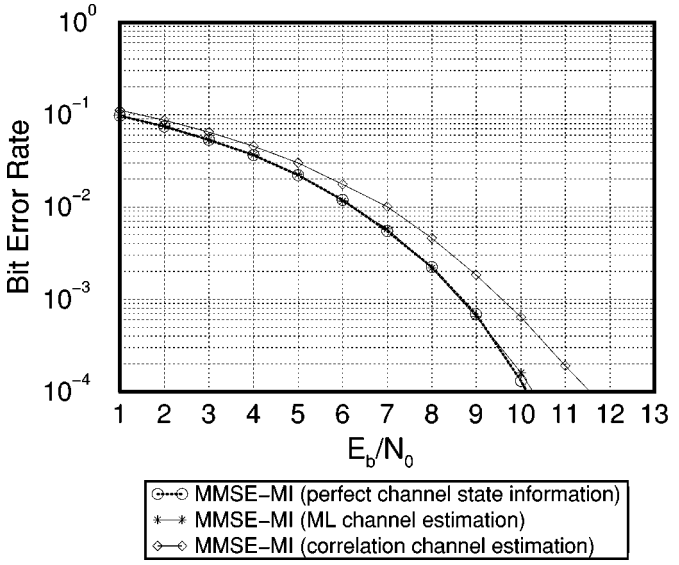

Fig. 9. BER performance comparison for the MMSE-MI detector assuming perfect channel state information and an estimated channel using two different algorithms. There are 5 active codes $(Q_1 = \cdots Q_5 = 16)$ and the oversampling factor is $\beta = 2$. [P. Castoldi, "*Multiuser Detection in CDMA Mobile Terminals*," to be published by Artech House, Norwood, MA, May 2002, reprinted with permission].

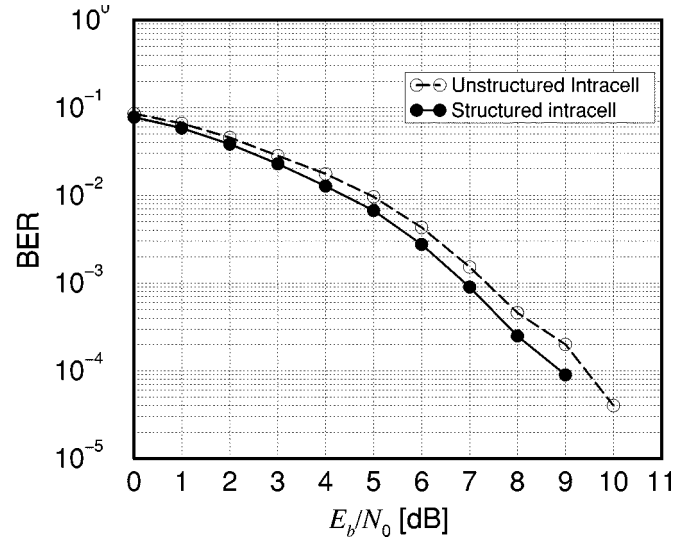

Fig. 10. Operating modes 1 and 2 for the MMSE-MI receiver, in a single cell scenario: BER performance comparison as a function of E_b/N_0. [P. Castoldi, "*Multiuser Detection in CDMA Mobile Terminals*," to be published by Artech House, Norwood, MA, May 2002, reprinted with permission].

to moderate loads $(\rho \leq 0.5)$ and it is almost equivalent to the single user lower bound. A performance degradation appears when the load is larger: see for example the case of $\rho = 0.875$.

In Fig. 9, we present the BER performance of the MMSE-MI detector as a function of the signal-to-noise ratio (SNR) in the presence of five data streams with spreading factor 16 and oversampling factor $\beta = 2$. In this case, matrix $\mathbf{F}$ is reconstructed using channel estimates obtained from the midamble of the data frame. Two channel estimation algorithms derived from [15] are considered: (1) a low-complexity channel estimation algorithm based on correlation, and (2) the least square estimator that attains asymptotically the Cramer Rao lower bound, implemented by a cost-effective discrete Fourier transform (DFT) technique. We can notice that the proposed detectors are sensitive to channel estimation error caused by the bias inherent in the correlation estimation algorithm. For an equal BER, the performance attained by the correlation estimation algorithm is worse by 1.3 dB with respect to the curves obtained with the least square channel estimator. In the latter case the performance is very close to the ideal case where the channel state information is perfectly known.

In Fig. 10, we present the comparison between the performance of the MMSE-MI receiver operated according to modes 1 and 2, described in Section IV, in a single-cell scenario. We

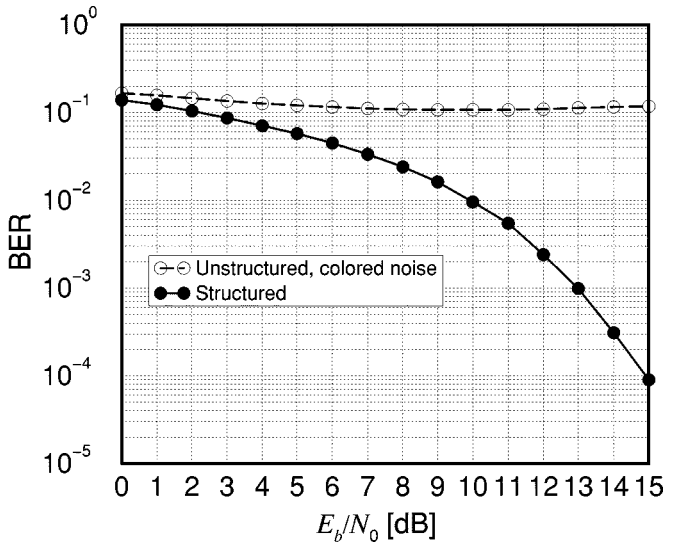

Fig. 11. Operating modes 3 and 4 for the MMSE-MI receiver, in a two cell scenario at the border of the desired cell: BER performance comparison as a function of E_b/N_0. [P. Castoldi, "*Multiuser Detection in CDMA Mobile Terminals*," to be published by Artech House, Norwood, MA, May 2002, reprinted with permission].

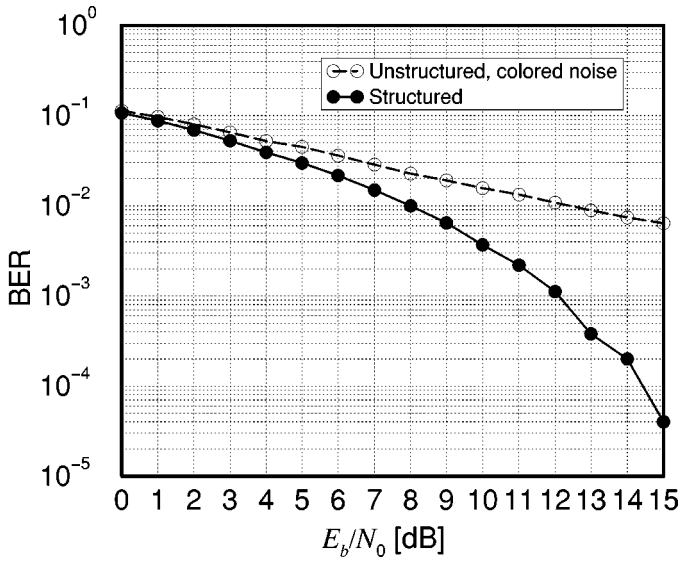

Fig. 12. Operating modes 3 and 4 for the MMSE-MI receiver, in a two cell scenario close to the border of the desired cell: BER performance comparison as a function of E_b/N_0. [P. Castoldi, "*Multiuser Detection in CDMA Mobile Terminals*," to be published by Artech House, Norwood, MA, May 2002, reprinted with permission].

have considered three active codes, whose spreading factors are $Q_1 = 4, Q_2 = Q_3 = 8$. The performance refers to the detection of the fastest user (i.e., the one with $Q_1 = 4$), modeled using a structured description whereas the other two codes are treated as colored noise according to model (18). We can see only a small degradation in the performance using unstructured approach (mode 2), which offers a strong complexity reduction with respect to the fully structured approach (mode 1).

C. Multiple Cell BER Performance

In Figs. 11 and 12, we have considered a two-cell scenario, where in each cell three codes, with spreading factors $Q_1 = 4, Q_2 = Q_3 = 8$, are active.

Fig. 11 compares the performance of the MMSE-MI receiver operated according to modes 3 and 4 exactly on the border of the cell of interest ($l = 0$, i.e., handover scenario), where the powers of the two BS are equals. It is evident that in this case the receiver performing direct mitigation of both intracell and intercell interference (receiver type 4) is the best. The use of the other receiver is completely impractical in such a situation.

Fig. 12 shows a comparison similar to the previous one, with the MS at a distance of $l = 40$ meters, from the cell boundary, which yields a $l/r\% = 8\%$. A superior performance of the structured operating mode (mode 4) is still evident, although the receiver of mode 3, based on unstructured model, performs better than in the previous situation.

VIII. Conclusion

We have considered different levels of abstractions in the description of both intracell and intercell interference which affect the downlink received signal of a multiple-cell multirate CDMA system. Specifically, we have proposed a tunable complexity description of the received signal by identifying two components in it: a structured part, containing the most significant part of the signal (either for detection or its rejection as interference) and an unstructured part, which essentially can be treated as Gaussian colored noise and is only statistically described.

Based on the above philosophy, we have proposed four "all-linear" receiver schemes using the ZF and MMSE criterion to counteract simultaneously both ISI and MAI. The proposed receivers are grouped into two families: (1) the first family of receivers restore separation of users by mitigating both ISI and MAI simultaneously; (2) the second family attempts to restore the orthogonality of the codes by simply equalizing the common channel (to eliminate ISI) and relies on a conventional detector for user separation. A relevant sliding window algorithm synchronized with the symbol rate of the slowest data stream is proposed and its fine structure is illustrated.

Theoretical BEP and simulation-based BER analysis have been conducted. A structured interference rejection is necessary to warrant a good detection performance especially in a multiple-cell scenario whenever the intercell interference is large, e.g., in a soft hand-over procedure. The single-cell scenario is less critical, the performance of the detectors approaches that of the single user lower bound, for both perfect and estimated channel state information, and it is nearly independent of the set of active codes up to moderate system loads.

Appendix I
Estimation of the Intercell Interference Parameters

If the term $\mathbf{n}(i)$ has a power $\sigma^2_{\mathbf{n}}$ significantly larger than the AWGN power $\sigma^2_{\mathbf{v}}$ and, simultaneously, its value is a large fraction of the global signal power $\sigma^2_{\mathbf{y}}$, we are in the presence of significant intercell interference. Intercell interference is always cyclostationary if the samples are given by data field contribution (as opposite to midamble samples). The power of the observation samples can be estimated as: $\hat{\sigma}^2_{\mathbf{y}} = (1)/(\beta N)\|\mathbf{y}(i)\|^2$. It is useful to estimate the power of the interfering signal in the

midamble of the desired signal were we perfectly know its structure; an estimation of the interference plus noise signal can be obtained by

$$\hat{\mathbf{n}}(i) = \mathbf{y}(i) - \mathbf{F}_d(i)\mathbf{b}_d(i) \tag{74}$$

since the MS can detect all the active midamble sequences and power estimation is given by $\hat{\sigma}^2_{\mathbf{n}} = (1)/(\beta N)\|\hat{\mathbf{n}}(i)\|^2$. We can then estimate the power of the intercell interference as $\hat{\sigma}^2_{\mathbf{z}} = \hat{\sigma}^2_{\mathbf{n}} - \hat{\sigma}^2_{\mathbf{v}}$.

For estimation of the correlation matrix $\mathbf{R}_{\mathbf{n}}(i)$, we make the assumption that the co-channel interference due to other MSs of neighboring cells is negligible and we assume that only interference of other BSs is significant. The samples of the process $\mathbf{n}(i)$ can be recovered using (74) on a proper window. To this purpose we define the vector $\hat{\mathbf{n}}_m = \hat{\mathbf{n}}^{(Q_{\max}+P-1)}(mQ_{\max} + P - 1)$. Hence, $\mathbf{R}_{\mathbf{n}}$ can be estimated from the received signal by averaging in the following way:

$$\hat{\mathbf{R}}_{\mathbf{n}} = \frac{1}{M}\sum_{m=1}^{M} \hat{\mathbf{n}}_m \cdot \hat{\mathbf{n}}_m^H. \tag{75}$$

APPENDIX II
EXACT EXPRESSION OF THE CORRELATION MATRIX $\mathbf{R}_{\mathbf{n}}(i)$

If we assume that the structure of the interference is known perfectly, we can evaluate the autocorrelation of the global interference as follows:

$$\begin{aligned}\mathbf{R}_{\mathbf{n}}(i) &= E\left[\left(\sum_{\lambda=1}^{L}\mathbf{F}_\lambda\mathbf{b}_\lambda(i) + \mathbf{v}(i)\right)\right.\\ &\qquad\left.\times\left(\sum_{\kappa=1}^{L}\mathbf{F}_\kappa\mathbf{b}_\kappa(i) + \mathbf{v}(i)\right)^H\right]\\ &= \sum_{\lambda=1}^{L}\sum_{\kappa=1}^{L}\mathbf{F}_\lambda\mathbf{R}_{\mathbf{b}_{\lambda,\kappa}}(i)\mathbf{F}_\kappa^H + \sigma^2_{\mathbf{v}}\mathbf{I}_{\beta N}\end{aligned} \tag{76}$$

where $\mathbf{R}_{\mathbf{b}_{\lambda,\kappa}}(i) \triangleq E[\mathbf{b}_\lambda(i)\mathbf{b}_\kappa^H(i)]$ can be evaluated in closed form.

After some manipulations, we obtain

$$\begin{aligned}\mathbf{R}_{\mathbf{n}}(i) &= \sum_{\lambda=1}^{L}\sum_{\kappa=1}^{L}\begin{Bmatrix}\sigma^2_{\mathbf{a}_\lambda}\mathbf{F}_\lambda\mathbf{C}_\lambda(i)\mathbf{C}_\lambda^H(i)\mathbf{F}_\lambda^H\delta_{\lambda,\kappa}\\ \mathbf{F}_\lambda\mathbf{b}_\lambda(i)\mathbf{b}_\kappa^H(i)\mathbf{F}_\kappa^H\\ 0\end{Bmatrix} + \sigma^2_{\mathbf{v}}\mathbf{I}_{\beta N}\\ &\approx \sum_{\lambda=1}^{L}\begin{Bmatrix}\sigma^2_{\mathbf{a}_\lambda}\mathbf{F}_\lambda\mathbf{F}_\lambda^H\\ \mathbf{F}_\lambda\mathbf{b}_\lambda(i)\mathbf{b}_\kappa^H(i)\mathbf{F}_\kappa^H\\ 0\end{Bmatrix} + \sigma^2_{\mathbf{v}}\mathbf{I}_{\beta N}\end{aligned} \tag{77}$$

where $\delta_{\lambda,\kappa}$ is the Kronecker delta. The upper line of (77) accounts for crosscorrelation of data-like interferers, the second line accounts for crosscorrelation of midamble-like interferers, while the third line applies for crosscorrelation between a midamble-like and a data-like interferer (assuming a zero mean value of the constellation symbols).

REFERENCES

[1] Radio Interface Technical Specifications [Online]. Available: http://www.3gpp.org

[2] M. Haardt, A. Klein, R. Koehn, S. Oestreich, M. Purat, V. Sommer, and T. Ulrich, "The TD-CDMA based UTRA-TDD mode," *IEEE J. Select. Areas Commun.*, vol. 18, pp. 1375–1385, Aug. 2000.

[3] I. Ghauri and D. Slock, "Linear receivers for the DS-CDMA downlink exploiting orthogonality of spreading sequences," presented at the 32nd Asilomar Conf. Sig., Syst. and Comp., Pacific Grove, CA, Nov. 1998.

[4] P. Castoldi and H. Kobayashi, "Intracell and intercell interference mitigation detectors for multirate transmission in TD-CDMA 3g systems," presented at the Africom 2001, South Africa, May 2001.

[5] ——, "Low complexity group detectors for multirate transmission in TD-CDMA 3G systems," presented at the Wireless Broadband Symposium (Globecom 2000), San Francisco, CA, Nov. 2000.

[6] U. Mitra, "Comparison of maximum likelihood-based detection for two multi-rate access schemes for CDMA signals," *IEEE Trans. Commun.*, pp. 64–77, Jan. 1999.

[7] H. Holma, S. Heikkinen, O.-A. Lehtinen, and A. Toskala, "Interference considerations for the time division duplex mode of the UMTS terrestrial radio access," *IEEE J. Select. Areas Commun.*, vol. 18, pp. 1386–1393, Aug. 2000.

[8] S. Verdù, *Multiuser Detection*. New York: Cambridge University Press, 1998.

[9] A. Høst-Madsen and K.-S. Cho, "MMSE/PIC multiuser detection for DS/CDMA systems with inter- and intra-cell interference," *IEEE Trans. Commun.*, vol. 47, pp. 291–299, Feb. 1999.

[10] A. Klein, G. Kaleh, and P. Baier, "Zero forcing and minimum mean-square-error equalization for multiuser detection in code division multiple-access channels," *IEEE Trans. Veh. Technol.*, vol. 45, pp. 276–287, May 1996.

[11] A. Klein and P. Baier, "Linear unbiased data estimation in mobile radio systems applying CDMA," *IEEE J. Select. Areas Commun.*, vol. 11, pp. 1058–1066, Sept. 1993.

[12] A. Klein, G. Kaleh, and P. Baier, "Equalizers for multiuser detection in code division multiple access mobile radio systems," in *Proc. Vehicular Technology Conf. (VTC'94)*, pp. 762–766.

[13] A. Klein, "Data detection algorithms specially designed for the downlink of CDMA mobile radio receivers," in *Vehicular Technology Conference (VTC'97)*, Phoenix, AZ, May 1997, pp. 203–207.

[14] H. V. Poor and S. Verdù, "Probability of error in MMSE multiuser detection," *IEEE Trans. Inform. Theory*, vol. 43, pp. 858–871, May. 1997.

[15] B. Steiner and P. Jung, "Optimum and suboptimum channel estimation for the uplink of CDMA mobile radio systems with joint detection," *Eur. Trans. Telecommun.*, vol. 5, pp. 39–50, Jan.–Feb. 1994.

[16] P. Castoldi and R. Raheli, "On recursive optimal detection of linear modulation in the presence of random fading," *Eur. Trans. Telecommun.*, vol. 9, no. 2, pp. 209–220, Mar./Apr. 1998.

[17] N. J. Fliege, *Multirate Digital Signal Processing*. New York: Wiley, 1994.

[18] C. W. Therrien, *Discrete Random Signals and Statistical Signal Processing*. Englewood Cliffs, NJ: Prentice-Hall, 1992.

[19] R. N. McDonough and A. D. Whalen, *Detection of Signals in Noise*, 2nd ed. New York: Academic, 1995.

Piero Castoldi (S'93–A'96) was born in Trento, Italy, in 1966. He received the Dr.Ing. degree in electrical engineering (with honors) from the University of Bologna, Bologna, Italy, in 1991. He received the Ph.D. degree in information engineering from the University of Parma, Parma, Italy, in 1996.

He spent one year as a Post-Doc at Princeton University and he has regular summer appointments at Princeton University, NJ, since 1998. From 1998 to 2001, he was an Assistant Professor at University of Parma. Since 2001, he has been Associate Professor of Telecommunications at Scuola Superiore Sant'Anna of Pisa, Pisa, Italy. Currently, he coordinates the broadband communications Laboratory at Scuola Superiore Sant'Anna and his research interests include receiver design for mobile radio communications and network aechitectures for multimedia services. He is author of more than 20 technical papers in refereed journals and conferences and of a textbook on multiuser detection in CDMA mobile terminals. He is also managing four national projects in the area of wireless broadband communications and interconnection of heterogeneous networks.

Hisashi Kobayashi (S'66–M'68–SM'76–F'96) received the B.E. and M.E. degrees in electrical engineering from the University of Tokyo, in 1961 and 1963, and the Ph.D. degree from Princeton University, NJ, in electrical engineering, in1967.

He is the Sherman Fairchild University Professor of Electrical Engineering and Computer Science at Princeton University, NJ, since 1986, when he joined the Princeton faculty as the Dean of the School of Engineering and Applied Science (1986–1991). From 1967 to 1982, he was with the IBM Research Center in Yorktown Heights, and from 1982 to 1986 he served as the founding Director of the IBM Tokyo Research Laboratory. He was a radar designer at Toshiba Corporation, Kawasaki, Japan, from 1963 to 1965. His research experiences include radar systems, high speed data transmission, seismic signal processing, coding for high density digital recording, image compression algorithms, performance modeling and analysis of computers and communication systems, and VLSI design algorithms. His current research interests include performance modeling and analysis of high-speed networks, wireless communications, and geolocation algorithms, optical network reliability and security, and teletraffic and queueing theory. He has authored more than 150 research articles, and has published a book "Modeling and Analysis" (Addison-Wesley, 1978), and is currently authoring a graduate-level textbook "*High speed Communication Networks, Vol. I: Modeling and Analysis Techniques*" (scheduled to be published by Prentice Hall in 2002).

Dr. Kobayashi was the recipient of the Humboldt Prize from Germany in 1979, the International Federation of Information Processing Silver Core Award in 1981, and the IBM Outstanding Contribution Awards in 1975 and 1984. He was elected a member of the Engineering Academy of Japan, in 1992.